2026 IEEE International Conference on Robotics and Automation (ICRA 2026)
June 1-5, 2026. Vienna, Austria

SIPHON: An Origami Soft Salp Robot

Brian Van Stratum† Nathan Justus Ross L. Hatton Joseph R. Davidson Geoffrey Hollinger

***Abstract*—We present SIPHON, a Salp-Inspired robot designed to utilize Passive Hydrodynamics, and equipped with soft robotic Origami bellows and soft Nozzles. We reveal the construction, including a novel use of an interlocking origami Kresling pattern, along with duckbill and mammal-heart-inspired valves. We derive a physical model for the coupled dynamics of body displacement and body contraction. We show experimental results of pool free swimming trials, and we compare these results to the model. Compared to other power-autonomous, bio-inspired pulsed jet swimmers, SIPHON swims with high speed and efficiency, achieving a mean swimming speed of $\mathbf{16.5}\,\mathrm{cm/s}$ ($\mathbf{0.59}\,\mathrm{Bl/s}$) and a cost of transport of $\mathbf{4.9}\,\mathrm{J/m}$ ($\mathbf{1.8}\,\mathrm{W\,s/(N\,m)}$).**

***Index Terms*—Bioinspiration, Swimming, Origami, Soft Robotics**

I. Introduction

Salps are tube-shaped gelatinous sea creatures that swim and eat by pulsing their body to move water [1]. Their simple body structure and ability to traverse long distances in the ocean make them exemplary for researchers seeking to encode insights from their unique life form into synthetic systems for locomotion and multi-agent interaction [2]. Salps benefit both from a simple chainable body form and the advantages of pulsed jets, which include rapid production of thrust [3], better cost of transport (CoT) both from having multiple jet sources smooth acceleration [4], and from being pulsed instead of continuous [5].

Salps are unique among other jet-propelled swimmers, such as squids, cuttlefish, and octopus, in that they draw water in their mouth and expel it out the back, producing a unidirectional flow (see Fig. 1a). Squid-like swimmers intake and expel water at their posterior, requiring flow direction reversal from forward to back. Froude efficiency analysis predicts that there are efficiency gains for salp-like unidirectional flow gaits as compared to the squid-like bidirectional flow gait [6], [7], and some salp-inspired robots have shown a 10.5% improvement associated with unidirectional flow in salp robots [8].

Previous works that have explored pulsed jet swimming have been focused on squid-like or bidirectional flow patterns [9] or focused on surface swimming [10], [11]. Surface swimming provides a useful gait demonstration but restricts the robot's domain of motion and introduces free-surface effects into the hydrodynamics.

Thanks to Magnolia, Chris Holm, and Evan Palmer for help running experiments. This work was funded in part by ONR awards N00014-22-1-2114 and N00014-23-1-2171.

† All authors are with the Collaborative Robotics and Intelligent Systems (CoRIS) group at Oregon State University in Corvallis, OR, USA
{vanstrab, ross.hatton, joseph.davidson, geoff.hollinger}@oregonstate.edu

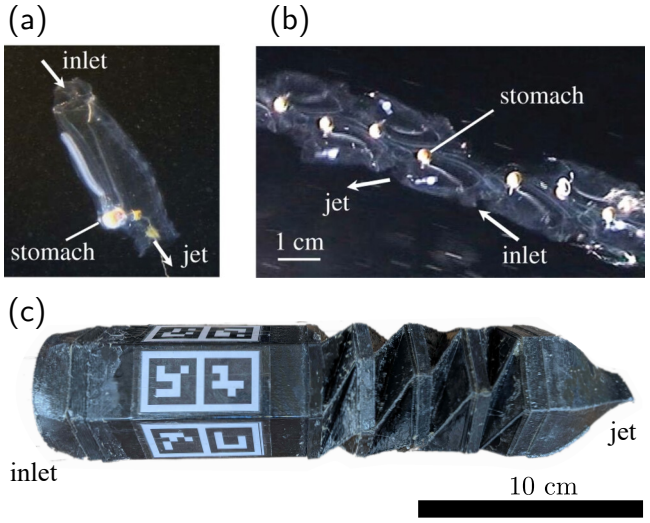

Fig. 1. (a) Weelia cylindrica oozooid (solitary form) (b) blastozooid stage (colony chain form). (c) Our salp-inspired soft robot with origami bellows and passive nozzles. (a) and (b) are adapted from [4]. Reprinted with permission from [The Royal Society].

Integrating origami into robot design offers the chance to encode complex motions directly into robot forms [10], [12]. The Kresling folding pattern in particular allows the efficient buckling of a cylindrical structure, effectively coupling rotation of the front and back pattern frames to a significant shortening of the structure [13]. Previous research has investigated using the Kresling cell as a bellows actuator [14]. Kresling cells are also known to produce thrust if they can be spun in the environment [15]. Recently, researchers have shown relatively high swimming speed with a centimeter-scale origami swimmer with artificial muscles, a buckling bellows, and a unidirectional flow gait [16].

In this work, we introduce SIPHON, a **S**alp **I**nspired **P**assive valve **H**ydrodynamic design equipped with soft robotic **O**rigami bellows and soft **N**ozzles. SIPHON is a simple and effective 3D printed design for exploring salp-inspired engineering, such as multi-agent control and fundamental physics, such as fluid-structure interaction. Moreover, noting a few exceptions [8], [16], SIPHON is unique in leveraging the advantages of salp-like unidirectional flow.

Salps in nature utilize some degree of peristalsis to achieve reversible propulsion [17]; SIPHON's unidirectional flow, in contrast, is achieved by a soft robotic technique of utilizing material stiffness in the form of 3D printed duckbill and heart-

inspired valves. SIPHON's flexible soft robotic design allows its inlet and jet valves to passively open or close based only on the balance of internal and external fluid pressure. This design choice simplifies the mechanism design and control, allowing SIPHON to be controlled with a single degree of freedom. SIPHON's waterproof bell and built-in data acquisition allow documentation of swimming speed and transport cost for free submerged swimming. Summarizing, the contributions of this paper are:

- Relative to untethered pulsed jet swimmers, we report low CoT with minimal mechanism and control complexity by utilizing passive hydrodynamics and material flexibility
- A novel 3D printed soft robotic salp design utilizing an origami Kresling pattern for the bellows
- Novel designs for 3D printed passively actuated mouth and tail nozzles
- Comparison of an analytical dynamic model that includes the effects of skin stiffness and motor power to experimental data
- Speed and CoT measurements for power autonomous submerged swimming with a unidirectional flow, salp-like gait

II. Modeling a Swimming Salp

Computational and analytical modeling for swimming organisms can be computationally expensive, especially when modeling the full fluid state, as in [18]–[20], or simpler, such as our own equation (6) for an effective nozzle. We desire a stateless fluid interaction model that is sufficiently complicated to capture the physics relevant to design and control. Inspired by both the coupled mass models that have given insight into the role of mode shapes and resonance in swimming [21], [22], we use the Euler-Lagrange method to derive coupled system dynamics that account for the jet pulse arising from body contraction due to DC motor torque.

Applying the Euler-Lagrange method to the coupled mass system and forces shown in Fig. 2 reveals equations of motion:

$$(m_b(s) + m_h)\ddot{x} + m_h\ddot{s} = F_j - F_d \tag{1}$$

$$m_h\ddot{x} + m_h\ddot{s} + b\dot{s} + 4k\,s = F_m - F_d + F_j \tag{2}$$

TABLE I
Model Parameters

Geometry & Mass				Design			
Parameter	Symbol	Value	Unit	Parameter	Symbol	Value	Unit
Head mass	m_h	339	g	Damping	b	800	N s/m
Bellows mass	m_b	337	g	Stiffness	k	250	N/m
Body frontal area	A	2827	mm^2	Rotation amplitude	Θ	29	rad
Nozzle area	A_n	79	mm^2	Control gain	k_p	0.05	N m/rad
Mouth area	A_m	336	mm^2	No-load speed	ω_{NL}	68	rad/s
Drag coefficient	C_d	4.0	-	Stall torque	τ_{stall}	70	N mm
Water density	ρ	1000	kg/m^3	Advance	k_{TR}	1.3	mm/rad
				Force radius	r	3.2	mm

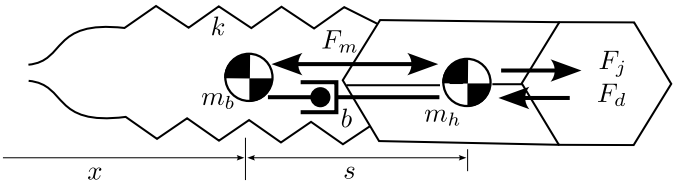

Fig. 2. Diagram of key variables for the analytical model: Bellows center of mass location x, bellows compression s, head and bellows mass m_b and m_h, damping coefficient b, motor force F_m, jet and mouth interaction force F_j, and drag force F_d.

Head and bellows masses are computed as the mass of the water within those volumes. If these volumes did not change shape, sucking and ejecting water, then added mass coefficients could be taken from a table such as [23]. However, because SIPHON swims by impelling and expelling water, a more complicated added mass analysis is left for future work. The motor control force F_m was computed using the same method implemented in hardware (see section III).

We define a control policy of the form $\tau_c = k_p\,(\theta_d - \theta)$ with a sinusoidal reference given by $\theta_d = \frac{\Theta}{2}\cos(2\,\pi\,f\,t) - \frac{\Theta}{2}$. Applied actuation torque τ is computed from the control torque τ_c by subjecting it to a linear motor saturation model given by $\tau_{max} = \tau_{stall}\,(1 - \omega/\omega_{NL})$. More motor model details are given in [24]. Motor shaft speed ω is computed from contraction speed and the lead screws advance as $\omega = 2\,\dot{s}/k_{TR}$. Generalized force associated with the motor force is $F_m = 2\,\tau/r$ where r is the effective radius of action for the linear screw. The required motor torque varied monotonically with the dissipative force b during the contraction and expansion phases. Thus, the b parameter was increased to match the experimental data in Fig. 6.

In order to model SIPHON's passive valving and switching, we model the thrust force Fj using a discontinuity based on the bellows contraction speed $\dot{s}$. We assume that the force in both cases can be computed as arising from continuity equations related to the body's internal volume. Here A is SIPHON's effective bellows frontal area for a diameter of 6 cm, A_n is the outlet jet nozzle described in section III, and A_m is the mouth's area estimated from mouth slit length and video of the slits as they open while swimming.

$$F_j(\dot{s}) = \begin{cases} 4\,\rho\frac{A^2}{A_n}\dot{s}^2 & \text{if } \dot{s} \le 0 \\ 4\,\rho\frac{A^2}{A_m}\dot{s}^2 & \text{if } \dot{s} > 0 \end{cases} \tag{3}$$

SIPHON's drag coefficient is complicated by the presence of the pulsed jet, the Kresling bellow's angular design, the unsteady motion of the pulsing bellows, the changing frontal area of the mouth valve, and the skin rotation arising from conservation of angular momentum. Despite these limitations, we represent drag using a constant dimensionless drag coefficient, C_d, noting that its value is understood as a bulk average for the gait. Thus, we model the drag force as only varying with head speed in the global frame as

$$F_d = \frac{1}{2}\,\rho\,A\,C_d(\dot{x} + \dot{s})^2\,\text{sgn}(\dot{x} + \dot{s}). \tag{4}$$

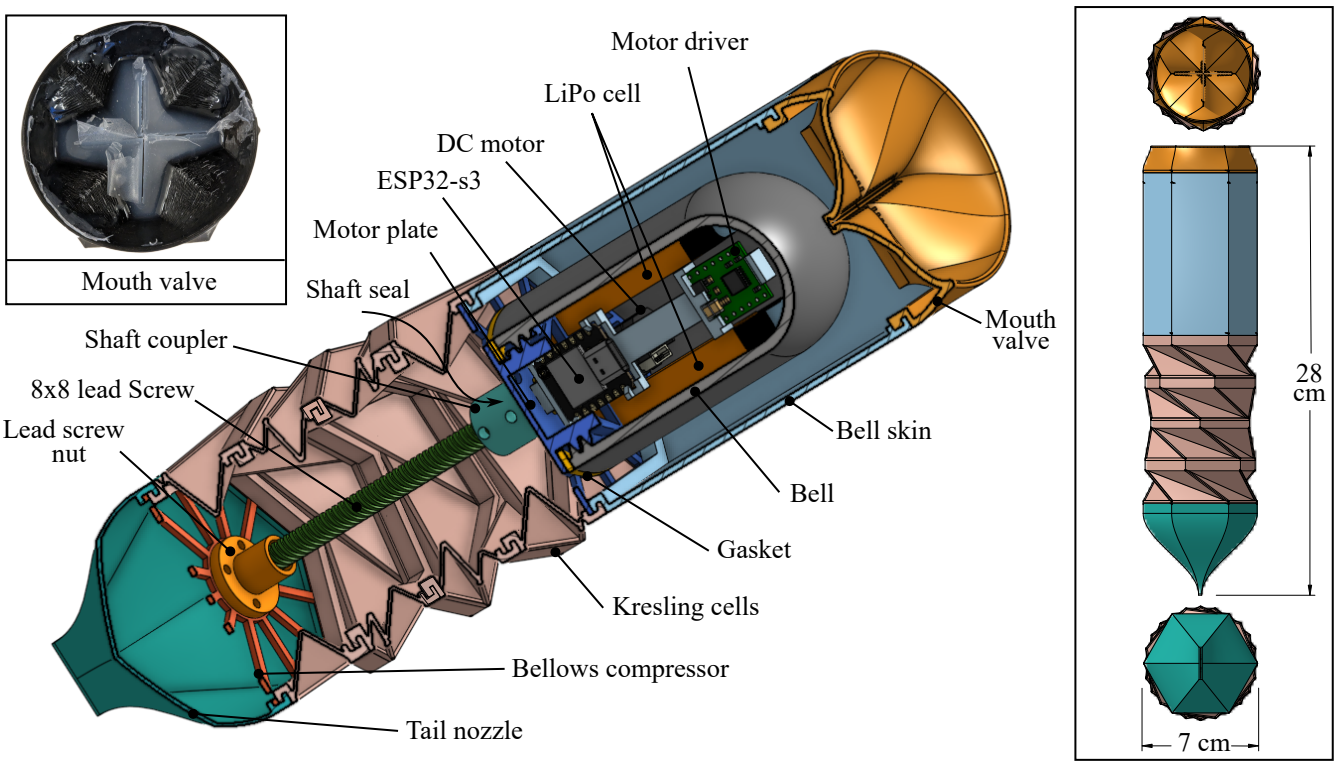

Fig. 3. (left) Detail of heart valve-inspired mouth valve after silicone pour and before trimming. (center) Section View of SIPHON robot. SIPHON's dry mass is 277 g. Mouth Kresling Cells and tail nozzles are made from 3D-printed TPU with a natural rubber latex treatment. The bell, bell skin, motor plate, and bellows compressor are made of 3D printed PLA. (right) Orthogonal views, including side, top, and bottom.

SIPHON's stride length varies monotonically with $1/C_d$, thus C_d was varied to produce a match with the experimental data in Fig. 5.

In order to visualize the model and compare it to experiments (see Fig. 5 and 6), we solve the equations of motion for acceleration. Then, after writing in first order form, we use MATLAB's built-in ODE45 solver to get solutions to the initial value problem [25].

III. Building SIPHON

Salps in nature can be found in colonial chain structures [26]. We desire a modular soft salp design that is also chainable and modular. To achieve this goal, we propose a 3D-printed design that can be adapted for chaining and allows different sensor modules to be attached to the basic propulsion unit. SIPHON's cylindrical shape is based roughly on *W. Cylindrica*, which is among the faster salp species [27]. SIPHON is composed of a bell that waterproofs an actuating DC motor, power electronics, and a microcontroller. The bell and transmission are centrally located within a semisoft skin with passive one-way valves at the mouth and tail (see Fig. 3 center). This design pulls fluid into the mouth, between the bell and bell skin, and expels water out the tail nozzle in a jet during contraction. All flexible components are printed out of Ninjaflex TPU on a Prusa XL.

We equip SIPHON with a flexible salp-inspired oral siphon at the mouth inlet, as shown in Fig. 3 left. The particular shape of this valve is inspired by Mammalian tricuspid valves [28]. These allow the mouth to both open large and hold shut against flow reversal. During bellows expansion, low fluid pressure pulls this valve open to let water flow in. During this time, the mouth valve's multiple slits allow it to swing through a shorter radius, resulting in tighter bell clearance and eliminating the need for extra space, volume, and ultimately reducing virtual mass. During body compression, when internal pressure is high, the mouth valve closes, forming a seal that is augmented with a layer of EcoFlex silicone.

SIPHON's bell waterproofs a Pololu Hi Power Carbon Brush motor with a 50:1 gearhead and built-in encoder. A Xiao Seeed ESP32-S3 manages communication, datalogging, and the motor controller described in section II. A Pololu motor controller (DRV8874) supplies battery current to the motor, accepts PWM control from the ESP32, and provides current feedback for torque logging, as shown in Fig. 6.

Early prototype experiments with flexible nozzled swimmers showed that material buckling is a valuable property for generating propulsion [29]. The Kresling folding pattern provides a coupling between linear compression and rotation accompanied by predictable buckling. Though Kresling-like patterns exist for other polygons, a hexagon is selected for its unique packing properties, as in arrayed cylinders and honeycombs.

SIPHON's flexible bellows are constructed from Kresling cells with interlocking tongue-and-groove patterns. This approach allows easy manufacturing and assembly of the

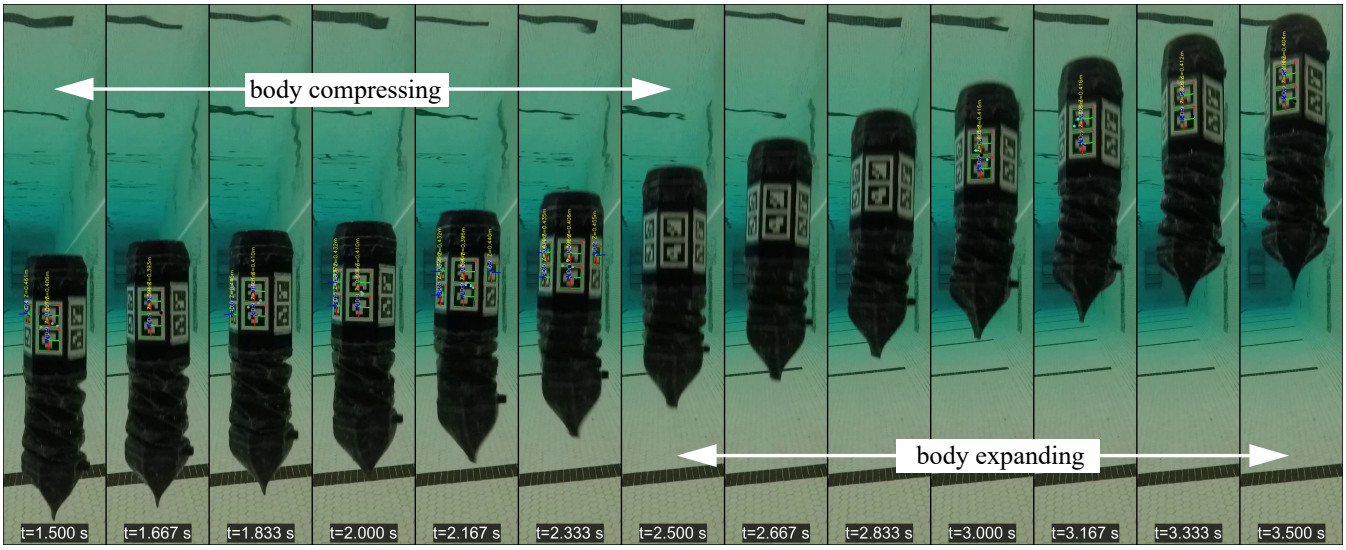

Fig. 4. Frames of free swimming experiment, pulsing at 0.5 Hz in OSU's Langdon Pool. Reference frames detected by the ArUco library are overlaid on their respective markers. Frames are evenly distributed across a single gait period, separated by twenty frames each.

Mouth, Bell skin, bellows, and tail nozzle. SIPHON's Kresling cells are 20 mm tall with hexagons inscribed inside 70 mm diameter circle, with a 0.8 mm wall thickness and 45° rotation between each frame. SIPHON's combined bellows stiffness was determined by applied load and measured displacement to be 250 N/m.

SIPHON's tail nozzle is a flat duckbill tapering to a slit opening to accommodate passive shutting during the expansion phase. As SIPHON contracts, the pressure inside the robot increases, shutting the mouth valve and simultaneously opening the tail nozzle. During this contraction phase, SIPHON's propulsion comes from fluid rapidly escaping the back, forming a jet. The jet nozzle is designed with a long, minimal curvature shape designed to reduce the fluid friction losses associated with interior flow over sharp-edged features as the jet escapes. Moreover, this smooth curvature enables streamlined flow over the outer skin as well, reducing flow separation and drag.

SIPHON's jet nozzle opening was chosen using a simple jet energy analysis. A stationary jet adds kinetic energy to its surroundings at a rate of $P_{jet} = \frac{1}{2}\dot{m}v_{jet}^2$. Applying continuity equations, we derive an expression in terms of bellows contraction rate, $\dot{L}$ body area, and nozzle area as

$$P_{jet} = \frac{\rho\, A^3}{2\, A_N^2}\dot{L}^3 \tag{5}$$

Noting that peak power generally occurs at half a motor's no-load speed, we write the contraction speed in terms of this shaft speed. If we assume that P_{jet} is supplied by a motor power P_{motor} reduced by transmission losses quantified by efficiency η, we can derive a nozzle diameter, D_n, that is matched to the motor's peak power.

$$D_n = \left(\frac{\pi\rho\, D^6\omega_{NL}^3\, K_{TR}^3}{64\,\eta\, P_{motor}}\right)^{\frac{1}{4}} \tag{6}$$

Plugging in parameters for SIPHON's body diameter and our motor and 50% efficiency, gives a jet diameter of 10 mm. Assuming the jet nozzle slit opens such that the slit length forms half a circumference, this defines the 18 mm nozzle width found on SIPHON.

IV. SIPHON's Speed and Cost of Transport

Unlike their biological analogs, many salp-inspired synthetic systems function as surface swimmers. A goal of this research was to quantify a salp-inspired swimmer's performance completely underwater. To quantify SIPHON's untethered free swimming, SIPHON was designed to be trimmable to slight negative buoyancy, with buoyancy adjustment achieved by adding graduated weights within the bell. SIPHON's free swimming experiments were in two large swimming pools (see Fig. 4) in approximately 120 cm of water depth and another pool in 95 cm of water.

Video was captured with a GoPro Hero 4 mounted to an aluminum 8020 frame. The camera was set to wide-angle at 1920×1080 pixels and recorded at 120 frames per second. Before testing, a calibration video was made with a checkerboard pattern in various positions. Markers were placed on the pool floor, marking out a 20 cm × 20 cm cross hair 50 cm back from the camera to return SIPHON for each swimming test.

SIPHON was placed in the pool and manually positioned in the designated region for each test. A test header message containing the requested pulse frequency, peak shaft rotation angle, and number of pulses was sent from a nearby laptop computer via a transponder made from a silicon-potted ESP32-s3 dev module utilizing the ESP-NOW Wi-Fi packet. Wi-Fi frequency radio signals attenuate significantly underwater, but data transmission was reliable when SIPHON and the transponder were within approximately 20 cm. Upon receipt of the data packet, SIPHON is programmed to execute the test

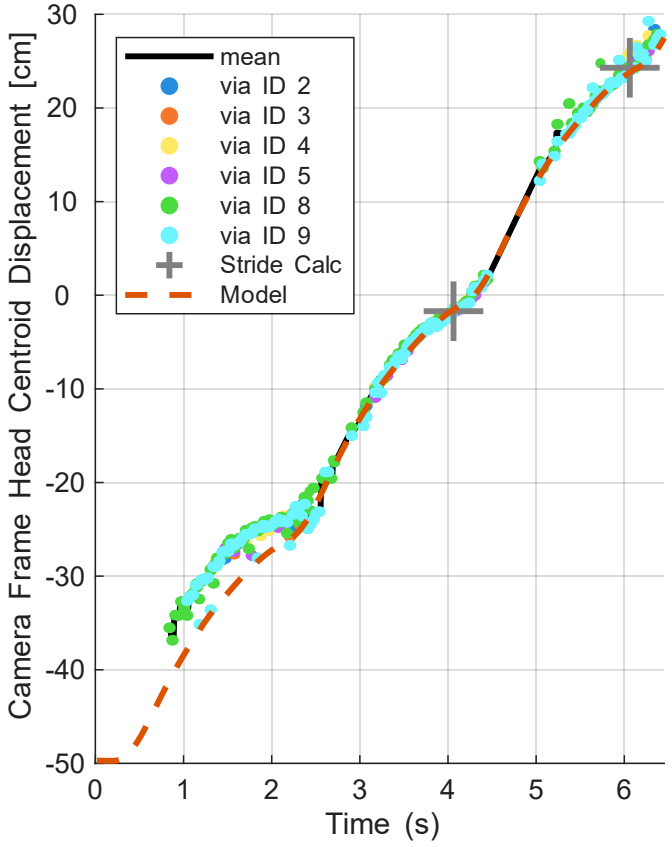

Fig. 5. Swimming marker capture and model overlay. See supplementary video. Colored points depict the head centroid location as projected by the marker ID shown. The Model is time-space shifted to align at the end of the first stride after the flow has time to develop in the experiment.

sequence while writing shaft speed and motor current data to memory at 400 Hz. At the end of the test, SIPHON sends the data back to the laptop via the same ESP-NOW packets, to the transponder, and to the laptop as binary values over serial USB, where they are recorded in a MATLAB structure. Four tests were run at randomized frequencies between 0.4 Hz to 0.9 Hz where SIPHON swam from the pool bottom to the surface. Use of the dense 8 by 8 lead screw and the hollow bell creates a significant distance between the CoM and center of buoyancy, this causes SIPHON to passively orient to vertical during free swimming tests.

SIPHON is equipped with twelve ArUco markers around its bell skin to facilitate underwater motion tracking. A Python script, utilizing the ArUco library in OpenCV [30], [31], extracts positions from video experiment records. The ArUco library reports position vector $\mathbf{P}$ and orientation of each marker in the camera's inertial reference frame I with origin point o at the camera. For tracking the head centroid's position at point c, c must be located relative to each marker location points m. The position vector that points from the i_{th} marker center m_i to the bell skin centriod c in the marker's local reference B_i is measured and stored as $\mathbf{P}^{B_i}_{m_i\,c} = \begin{bmatrix}\pm d & 0 & -r\end{bmatrix}^T$ where d is half the distance between the ArUco codes and r is the body radius. The matrix tensors $\mathbf{T}_{B_i \to I}$ that transform vectors from B to I are called from a built-in ArUco library function. Thus, in the inertial camera frame, if i markers are visible, centroid point location estimates c_i are given via $\mathbf{P}^I_{o\,c_i} = \mathbf{P}^I_{m_i} + \mathbf{T}_{B_i \to I}\mathbf{P}^{B_i}_{m_i\,c_i}$

Figure 5 shows the head centroid displacement measurements as reported by various marker IDs for SIPHON swimming at 0.5 Hz. The black "mean" trace is the mean of these locations in each frame. The gray crosses depict the time indices used to compute the stride length λ for this particular test. These are located by first selecting a final time index candidate t_f from which an initial time t_i is computed from the known pulse frequency f for the test $t_i = t_f - \frac{1}{f}$. Corresponding d_i and d_f are interpolated from the "mean" line. Finally, λ is computed as $d_f - d_i$, and the measured bias, as explained in the paragraph below, is subtracted. The mean swimming speed is computed as $\overline{v} = \lambda\, f$. The results of this method are displayed in Table II.

Power expended while swimming is recorded by the current as measured by the feedback sensor and the motor's shaft speed as measured by the incremental encoder. Thus, mechanical power output is computed as the absolute value of the product of speed and torque $P = \text{abs}(\tau\,\omega)$. We compute torque from the motor's torque-current relationship published by Pololu in their datasheet for the motor. After the test data is sent from SIPHON back to MATLAB, the time data vector with n pulses and SR sampling rate is reshaped as a $\frac{SR}{f} \times n$ matrix to compute typical gait waveform averages with MATLAB's mean function. Results of this analysis are shown in Fig. 6. Along with computing the average stride-wise waveforms, we also compute the absolute average mean power, shown as a black dashed line in Fig. 6 and reported for each experiment in Table II. The dimensionless CoT reported here is scaled by SIPHON's dry weight as $\text{CoT} = \overline{P}/(\overline{v}\,2.72\,\text{N})$. Here SIPHON's dry weight from a dry mass of 277 g scales the power output. Arguably, the dry mass plus the added mass, values of Table I, could have been used, which would improve the CoT.

Given the inherent challenges of underwater pose estimation, we sought to quantify and report the precision and accuracy of the stride-length measurements from ArUco motion tracking. To do this, the test apparatus was laid level on the ground, and a grade rod was positioned at 50 cm from the camera to match SIPHON's mean swimming line. Video was recorded while SIPHON's head was manually traversed along the grade rod, stopping approximately 5 s at 10 cm intervals. This data was manually clipped and labeled, and the results are shown

TABLE II
SUMMARY OF EXPERIMENTAL SWIMMING RESULTS

f Hz	$\overline{P}$ W	λ cm	$\overline{v}$ cm/s	$\overline{v}$ BL/s	CoT J/m	CoT W s/(N m)
0.4	0.70	32.8	13.1	0.47	5.33	2.0
0.5	0.75	23.5	11.8	0.42	6.37	2.3
0.6	0.80	27.5	16.5	0.59	4.85	1.8
0.9	1.33	17.9	16.1	0.58	8.24	3.0

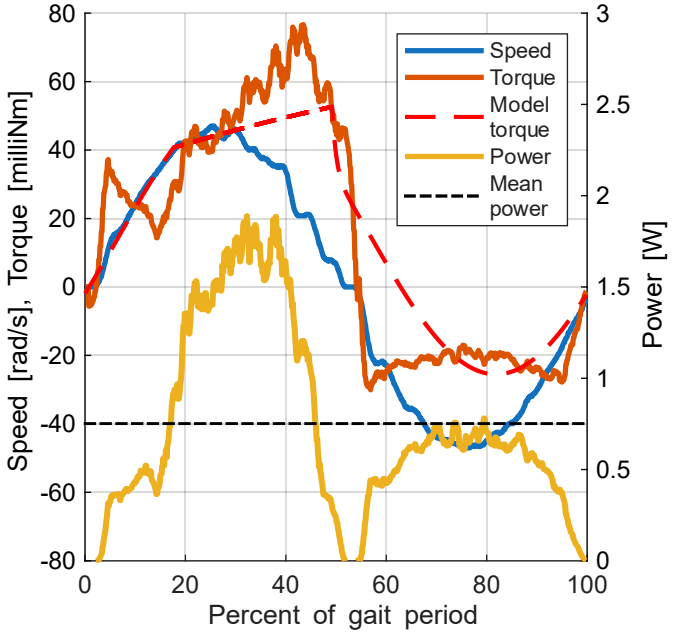

Fig. 6. Depiction of typical mean power output calculation (0.5 Hz shown here). Motor speed and torque as measured by the incremental encoder and current sensor. Output power is computed from the product of speed and torque and plotted on the right axis. The speed, torque, and power waveforms are gait-averaged. The black dashed line shown is the absolute mean power output. The red dashed line is an overlay of the motor torque from the computational model.

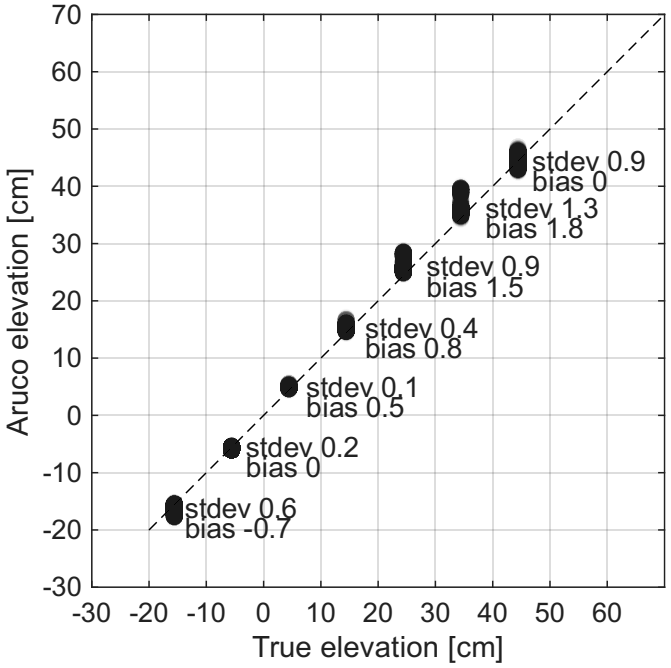

Fig. 7. Position Data confidence. stdev is a single standard deviation of the data at the point, and the bias is the vertical distance to the $y = x$ line.

in Figure 7. The bias associated with optical tracking, in the worst-case scenario, would overreport SIPHON's stride length by $1.8\,\mathrm{cm} - -0.7\,\mathrm{cm} = 2.5\,\mathrm{cm}$. Thus, we conclude that it is conservative to assume the worst and subtract this $2.5\,\mathrm{cm}$ from what is directly reported by the ArUco system. These bias-corrected measurements are reported in Tables II and III. From the noise in these measurements, we compute propagation of error for stride measurements as $\sqrt{1.3^2 + 0.6^2} = 1.4$ standard deviations, which amounts to $\pm 2.8\,\mathrm{cm}$ for a 95% confidence interval on stride length calculations.

V. Discussion and Future Work

This paper demonstrates that passive soft robotic compliance can be utilized to control fluid flow in a robotic jet-propelled swimmer with a single degree of freedom. The simplicity of SIPHON's design is of interest if one desires to produce power autonomous free-swimmers in larger numbers, since its components can be batch printed on 3D printers of moderate cost, and its minimal other components are readily obtained.

It seems that the traveling wave nature of salps' circumferential muscle activation is part of the success of their propulsion, and allows them to reverse travel direction by reversing this wave [17], [32]. Despite this, the success of these passive valves opens the question of the degree to which salps' forward locomotion utilizes this mechanism for passive actuation of their oral and atrial siphons.

This work has presented and evaluated locomotion speed and CoT as a function of actuation frequency. We are interested in several areas for future work, including the role of resonance in low-level design and the optimal control of these salp-inspired robots within the context of multi-agent interaction.

We have tabulated comparable pulsed jet swimmers' peak performance along with SIPHON's performance in Table III, showing that SIPHON's peak swimming performance is fast and efficient compared to other power autonomous pulsed jet free swimmers. Bujard and Weymouth's resonant swimmer outperforms SIPHON but is limited by its power tether in the former case, and pressure charging apparatus in the latter [21], [33]. These results bolster the computational and theoretical expectation [7], [19] of added performance from unidirectional flow gaits, with a concrete physical example of the effectiveness of passively actuated valves and nozzles.

TABLE III
Performance Comparison to Other Works

Robot	Speed (Bl/s)	CoT (W s/(N m))
Bujard et al. [21]	0.98 [a]	0.09
Chen et al. [16]	< 0.62 [b]	–
Christianson et al. [9]	0.54	–
SALP [11]	0.34	2.01
Salpot [8]	0.08	32.8
Weymouth et al [33]	10.0 [c]	–
Yang et al. [10]	0.20	2.0
SIPHON (this work)	0.59 ± 0.05	1.8 ± 0.1

[a] Tethered power supply
[b] Chen et al. report peak speed rather than time-averaged mean speed
[c] Charged and shot from a base station

REFERENCES

[1] Q. Bone and E. Trueman, "Jet propulsion in salps (tunicata: Thaliacea)," *Journal of Zoology*, vol. 201, no. 4, pp. 481–506, 1983.

[2] B. H. Abed-Alguni, D. Paul, and R. Hammad, "Improved salp swarm algorithm for solving single-objective continuous optimization problems," *Applied Intelligence*, vol. 52, no. 15, pp. 17 217–17 236, 2022.

[3] A. G. Athanassiadis and D. P. Hart, "Effects of multijet coupling on propulsive performance in underwater pulsed jets," *Phys. Rev. Fluids*, vol. 1, p. 034501, Jul 2016. [Online]. Available: https://link.aps.org/doi/10.1103/PhysRevFluids.1.034501

[4] K. R. Sutherland and D. Weihs, "Hydrodynamic advantages of swimming by salp chains," *Journal of The Royal Society Interface*, vol. 14, no. 133, p. 20170298, 2017.

[5] L. A. Ruiz, R. W. Whittlesey, and J. O. Dabiri, "Vortex-enhanced propulsion," *Journal of Fluid Mechanics*, vol. 668, pp. 5–32, 2011.

[6] E. J. Anderson and M. E. Demont, "The mechanics of locomotion in the squid loligo pealei: locomotory function and unsteady hydrodynamics of the jet and intramantle pressure," *Journal of Experimental Biology*, vol. 203, no. 18, pp. 2851–2863, 2000.

[7] R. M. Alexander, *Principles of animal locomotion*. Princeton university press, 2003.

[8] X. Dong, H. Chen, Z. Zhou, C. Ouyang, L. Hu, F. Zhang, B. Chen, and Z. Gan, "Salpot: A jet propulsion swimmer with scissor structure and bilateral apertures," *IEEE Robotics and Automation Letters*, 2024.

[9] C. Christianson, Y. Cui, M. Ishida, X. Bi, Q. Zhu, G. Pawlak, and M. T. Tolley, "Cephalopod-inspired robot capable of cyclic jet propulsion through shape change," *Bioinspiration & Biomimetics*, vol. 16, no. 1, p. 016014, dec 2020. [Online]. Available: https://dx.doi.org/10.1088/1748-3190/abbc72

[10] Z. Yang, D. Chen, D. J. Levine, and C. Sung, "Origami-inspired robot that swims via jet propulsion," *IEEE Robotics and Automation Letters*, vol. 6, no. 4, pp. 7145–7152, 2021.

[11] Z. Yang, Y. Zhang, M. Herbert, M.-y. A. Hsieh, and C. Sung, "Effect of jet coordination on underwater propulsion with the multi-robot salp system," in *Proceedings of the IEEE International Conference on Soft Robotics (RoboSoft)*. Lausanne, Switzerland: IEEE, 2025, pp. 1–8.

[12] J. Hu, H. Li, and W. Chen, "A squid-inspired swimming robot using folding of origami," *The Journal of Engineering*, vol. 2021, no. 10, pp. 630–639, 2021.

[13] R. Masana, A. S. Dalaq, S. Khazaaleh, and M. F. Daqaq, "The kresling origami spring: a review and assessment," *Smart Materials and Structures*, vol. 33, no. 4, p. 043002, Mar. 2024. [Online]. Available: http://dx.doi.org/10.1088/1361-665X/ad2f6f

[14] H. Zhou, J. Gao, Y. Chen, Z. Shen, H. Lv, and P. Sareh, "A quasi-zero-stiffness vibration isolator inspired by kresling origami," *Structures*, vol. 69, p. 107315, Nov. 2024. [Online]. Available: http://dx.doi.org/10.1016/j.istruc.2024.107315

[15] Q. Ze, S. Wu, J. Dai, S. Leanza, G. Ikeda, P. C. Yang, G. Iaccarino, and R. R. Zhao, "Spinning-enabled wireless amphibious origami millirobot," *Nature Communications*, vol. 13, no. 1, Jun. 2022. [Online]. Available: http://dx.doi.org/10.1038/s41467-022-30802-w

[16] W. Chen, S. Yang, C. Zhu, Y. Cheng, Y. Shi, C. Yu, and K. Liu, "Scalable jet swimmer driven by pulsatile artificial muscles and soft chamber buckling," *Advanced Materials*, p. 2503777, 2025.

[17] N. N. A. Ariffian, K. M. Swadling, M. Moteki, and N. H. A. Ishak, "An assessment of environmental and ecological drivers of salp blooms in the world's ocean," *Regional Studies in Marine Science*, vol. 77, p. 103718, 2024. [Online]. Available: https://www.sciencedirect.com/science/article/pii/S2352485524003517

[18] F. Renda, F. Giorgio-Serchi, F. Boyer, and C. Laschi, "Modelling cephalopod-inspired pulsed-jet locomotion for underwater soft robots," *Bioinspiration & biomimetics*, vol. 10, no. 5, p. 055005, 2015.

[19] X. Bi, H. Tang, and Q. Zhu, "Feasibility of hydrodynamically activated valves for salp-like propulsion," *Physics of Fluids*, vol. 34, no. 10, 2022.

[20] J. Wang, D. S. Weaver, and S. Tullis, "Simplified fluid-structure model for duckbill valve flow," *Journal of Pressure Vessel Technology, Transactions of the ASME*, vol. 134, no. 4, p. 041301, 2012.

[21] T. Bujard, F. Giorgio-Serchi, and G. D. Weymouth, "A resonant squid-inspired robot unlocks biological propulsive efficiency," *Science Robotics*, vol. 6, no. 50, p. eabd2971, 2021.

[22] E. Kanso and P. K. Newton, "Passive locomotion via normal-mode coupling in a submerged spring–mass system," *Journal of Fluid Mechanics*, vol. 641, pp. 205–215, 2009.

[23] R. D. Blevins, "Flow-induced vibration," *New York*, 1977.

[24] B. Van Stratum, K. Shoele, and J. E. Clark, "Pacific lamprey inspired climbing," *Bioinspiration & Biomimetics*, vol. 18, no. 4, p. 046013, 2023.

[25] MathWorks, "Matlab r2025a," https://www.mathworks.com/products/matlab.html, Natick, Massachusetts, USA, 2025, version 25.1 (R2025a).

[26] A. Damian-Serrano and K. R. Sutherland, "A developmental ontology for the colonial architecture of salps," *The Biological Bulletin*, vol. 245, no. 1, pp. 9–18, 2023.

[27] K. R. Sutherland and L. P. Madin, "Comparative jet wake structure and swimming performance of salps," *Journal of Experimental Biology*, vol. 213, no. 17, pp. 2967–2975, 2010.

[28] M. Mathur, W. D. Meador, M. Malinowski, T. Jazwiec, T. A. Timek, and M. K. Rausch, "Texas trivalve 1.0: a reverse-engineered, open model of the human tricuspid valve," *Engineering with computers*, vol. 38, no. 5, pp. 3835–3848, 2022.

[29] B. V. Stratum, "Encoding salp locomotion insights into soft robotic systems," 2025, mechanical Intelligence Workshop -ICRA 2025. [Online]. Available: https://drive.google.com/file/d/1LB9cw3eUQThGlW4sKM-JWW60JLTRaYFw/view

[30] S. Garrido-Jurado, R. Muñoz-Salinas, F. J. Madrid-Cuevas, and M. J. Marín-Jiménez, "Automatic generation and detection of highly reliable fiducial markers under occlusion," *Pattern Recognition*, vol. 47, no. 6, pp. 2280–2292, 2014.

[31] G. Bradski, "The OpenCV Library," *Dr. Dobb's Journal of Software Tools*, 2000.

[32] N. Ishak, N. A. B. Adam, and Z. Kassim, "A taxonomic revision of the genus thalia blumenbach, 1798; weelia yount, 1954; brooksia metcalf, 1918 (salpida: Salpidae) from east coast of peninsular malaysia," *Zootaxa*, vol. 4422, no. 4, pp. 451–477, 2018.

[33] G. Weymouth, V. Subramaniam, and M. S. Triantafyllou, "Ultra-fast escape maneuver of an octopus-inspired robot," *Bioinspiration & biomimetics*, vol. 10, no. 1, p. 016016, 2015.